Geochimica et Cosmochimica Acta 337 (2022) 82–94

Contents lists available at ScienceDirect

Geochimica et Cosmochimica Acta

journal homepage: www.elsevier.com/locate/gca

The effect of CO_2 concentration on carbon isotope discrimination during photosynthesis in *Ginkgo biloba*: implications for reconstructing atmospheric CO_2 levels in the geologic past

Mason A. Scher [a,b,*], Richard S. Barclay [a], Allison A. Baczynski [c], Bryton A. Smith [a,1], James Sappington [d,2], Lily A. Bennett [d,e], Suvankar Chakraborty [f], Jonathan P. Wilson [e], J. Patrick Megonigal [d], Scott L. Wing [a]

[a] Department of Paleobiology, National Museum of Natural History, Smithsonian Institution, Washington, D.C, United States
[b] Chemistry Department, Drew University, Madison, NJ, United States
[c] Department of Geosciences, Pennsylvania State University, University Park, PA, United States
[d] Smithsonian Environmental Research Center, Edgewater, MD, United States
[e] Department of Environmental Studies, Haverford College, Haverford, PA, United States
[f] Stable Isotope Ratio Facility for Environmental Research (SIRFER), University of Utah, Salt Lake City, UT, United States

ARTICLE INFO

Article history:
Received 9 February 2022
Accepted 24 September 2022
Available online 2 October 2022
Associate editor: Aaron F Diefendorf

Keywords:
Carbon isotopes
Discrimination
Atmospheric CO_2 concentration
Paleo-pCO_2 proxy

ABSTRACT

Some experiments and observations of free-living plants have found that increasing atmospheric concentration of CO_2 (pCO_2) is directly correlated with increasing discrimination against ^{13}C during photosynthesis ($\Delta^{13}C$) in C3 plants. The inverted form of this correlation has been used to estimate pCO_2 in the geological past (i.e. the C3 plant proxy), but there has been little experimental work to establish the relative importance of pCO_2 as a driver of discrimination in more natural settings and over a range of pCO_2 relevant to the deep-time geologic record. Here we report on an experiment exploring the relationship between pCO_2 and $\Delta^{13}C$ in *Ginkgo biloba*, a plant long used to infer past CO_2 levels because of the strong similarity of extant to fossil *Ginkgo* and the abundance of *Ginkgo* fossils with preserved cuticle from late Mesozoic and Cenozoic periods of warm global climate.

We grew *Ginkgo biloba* plants for three years under ambient pCO_2 (~425 ppm) and elevated levels (~600, ~800, and ~ 1000 ppm) while measuring the carbon isotope composition of air ($\delta^{13}C_{air}$) and leaves ($\delta^{13}C_{leaf}$) as well as the ratio of internal to external CO_2 concentration (c_i/c_a), maximum photosynthetic assimilation rate (A_{max}), C:N ratio, and leaf mass per area (LMA). We found no significant relationship between pCO_2 and $\Delta^{13}C_{leaf}$ or c_i/c_a. We did find a direct correlation of pCO_2 with A_{max}, LMA, and C:N ratio. The lack of increase in $\Delta^{13}C_{leaf}$ with rising pCO_2 may result from the lack of change in c_i/c_a, thicker leaves that slow the rate of diffusion of CO_2 through the leaf to mesophyll cells, higher A_{max} that drives more rapid consumption of intracellular CO_2 and/or changes in the relative proportions of starches, lipids or other compounds that have distinct isotopic compositions.

Our results, along with a compilation of data from the literature on $\Delta^{13}C_{leaf}$ in many different types of C3 plants, suggest that $\Delta^{13}C_{leaf}$ does not consistently increase with increasing pCO_2. Rather, there is a diversity of responses, both positive and negative, that are not clearly related to taxonomic group or growth form but may reflect changes in leaf structure, stomatal response and A_{max} under higher pCO_2. Given the complex relationship between $\Delta^{13}C_{leaf}$ and pCO_2 in living plants we consider $\Delta^{13}C_{leaf}$ of fossil plants to be an unreliable proxy for paleo-atmospheric pCO_2.

© 2022 The Authors. Published by Elsevier Ltd. This is an open access article under the CC BY-NC-ND license (http://creativecommons.org/licenses/by-nc-nd/4.0/).

1. Introduction

Attempts to reconstruct the relationship between climate change and atmospheric carbon dioxide (pCO_2) in the geological past have led the earth science community to develop many proxies for pCO_2 that can be applied to periods before the oldest direct records of atmospheric composition from bubbles trapped in ice

* Corresponding author at: Department of Geosciences, Princeton University, Guyot Hall, Princeton, New Jersey, 08544, United States.
E-mail address: mscher@princeton.edu (M.A. Scher).
[1] Present address: Department of Earth & Environmental Sciences, Wesleyan University, Middletown, CT, United States.
[2] Present address: Chemistry Department, University of Virginia, Charlottesville, VA, United States.

https://doi.org/10.1016/j.gca.2022.09.033
0016-7037/© 2022 The Authors. Published by Elsevier Ltd.
This is an open access article under the CC BY-NC-ND license (http://creativecommons.org/licenses/by-nc-nd/4.0/).

(Petit et al., 1999; Siegenthaler et al., 2005; Lüthi et al., 2008; Petit & Raynaud, 2020). Testing and improving these geological proxies for pCO_2 is important because accurate estimates of paleo-pCO_2 will help reveal the role of high pCO_2 in maintaining hothouse climates, in feedbacks between the climate and carbon cycle, and the sensitivity of the Earth's climate to the addition of CO_2 to the atmosphere. Using Earth history to understand these interactions requires a reliable, stratigraphically dense proxy for pCO_2, yet currently there is quite large disagreement among different types of proxy estimates for the Cenozoic, as well as low stratigraphic density (Beerling & Royer, 2011; Royer, 2015; Westerhold et al., 2020).

One previously proposed proxy for paleo-pCO_2 relies on the firmly established preference of C3 plants for the light isotope of carbon. Plant tissues are depleted in the heavy isotope of carbon (^{13}C) relative to the atmosphere because they preferentially incorporate light carbon (^{12}C) into their tissues during photosynthesis. Farquhar et al. (1980, 1989a) suggested a simplified model for the carbon isotope discrimination between plant tissues and the surrounding atmospheric CO_2 (Eq. (1)),

$$\Delta^{13}C_{leaf} = a + (b - a)\left(\frac{c_i}{c_a}\right) \quad (1)$$

where "a" is the fractionation during diffusion into the stomata (4.4 ‰), "b" is the fractionation during carbon fixation due to RuBisCO (~27 ‰), c_i is the intercellular concentration of CO_2 within the leaf, and c_a is the concentration of CO_2 in the air around the leaf. (Note: Earth scientists commonly denote the atmospheric concentration of CO_2 as pCO_2, whereas plant physiologists refer to the concentration of CO_2 in the atmosphere around the leaf as c_a. Here we will use pCO_2 when referring to the general atmospheric concentration of CO_2 in the past and present, but c_a when referring to the atmosphere just external to the leaf.) CO_2 diffuses through stomata into the interior air spaces of the leaf prior to photosynthesis (see Fig. 1), so the value of c_i cannot exceed that of c_a. Observed c_i/c_a commonly ranges between 0.2 and 0.9. As the value of c_i/c_a approaches 1, the value of $\Delta^{13}C_{leaf}$ approaches that of fractionation by RuBisCO, or ~ 27 ‰. As c_i/c_a approaches 0, the value of $\Delta^{13}C_{leaf}$ from the Farquhar equation approaches that of fractionation during diffusion, or 4.4 ‰. Though the simplified Farquhar model focuses on the ratio c_i/c_a, which is controlled by stomatal conductance, it is important to note that fixation of carbon by RuBisCO occurs within chloroplasts, whose CO_2 concentration is denoted as c_c. Diffusion of CO_2 from substomatal spaces to chloroplasts via mesophyll conductance (g_m) is also known to play an important role in discrimination in many plants (Veromann-Jürgenson et al. 2020) which we consider in the discussion of our results. The value of $\Delta^{13}C_{leaf}$ can be calculated using measurements of the isotopic compositions of the air ($\delta^{13}C_{air}$) and the plant tissue ($\delta^{13}C_{leaf}$) with Eq. (2).

$$\Delta^{13}C_{leaf} = \frac{\delta^{13}C_{air} - \delta^{13}C_{leaf}}{1 + (\delta^{13}C_{leaf}/1000)} \quad (2)$$

Schubert and Jahren (2012) found a direct correlation of $\Delta^{13}C$ with pCO_2 in growth chamber studies of two herbaceous C3 species, *Arabidopsis thaliana* (thale cress) and *Raphanus sativus* (radish), under 15 levels of pCO_2 from 370 to 2255 and 407–4200 ppm, respectively. Light, temperature, relative humidity, soil moisture, and pCO_2 were all maintained at uniform levels in growth chambers in Schubert & Jahren, 2012, henceforth SJ2012. SJ2012 observed a positive hyperbolic relationship between $\Delta^{13}C$ and pCO_2 for bulk above-ground tissue (*R. sativus* and *A. thaliana*), bulk below-ground tissue (*R. sativus*), and *n*-alkanes (*A. thaliana*). They also compiled $\Delta^{13}C$ measurements from a number of prior studies of C3 plants growing under varying pCO_2 and argued these were consistent with the same hyperbolic relationship in which $\Delta^{13}C$ increases rapidly as pCO_2 increases from 0 to ~ 1000 ppm, then asymptotically to 28–30 ‰ as pCO_2 rises to 4000 ppm and fractionation due to RuBisCO is fully expressed. SJ2012 used this hyperbolic relationship to calculate sensitivity (S), the amount that $\Delta^{13}C$ increases with a given increment of pCO_2, by taking the derivative of a hyperbolic curve fit to their data. S is expressed in parts per mil per 100 ppm increase in pCO_2. SJ2012 calculated S values from the literature by fitting data with a hyperbolic equation and using the derivative of this curve to yield an S value. A compilation of these values was used to construct a relationship between pCO_2 and S. In a subsequent paper Schubert & Jahren (2015) offered an equation based on this hyperbolic relationship by which one can use $\Delta^{13}C$ from fossil organic matter to reconstruct paleo-pCO_2, provided we know the pCO_2 level at a reference time t = 0. This proxy has since been applied to a variety of geological data sets (Schubert & Jahren, 2015; Cui & Schubert, 2017; Cui et al., 2020; Wu et al., 2021).

Following the initial development and implementation of the C3 plant proxy, complicating factors have been recognized. SJ2012 already recommended that the C3 plant proxy should be applied only if the fossil plants for which $\Delta^{13}C$ was being estimated had grown in well-watered paleoenvironments, because water availability could change discrimination independently of pCO_2.

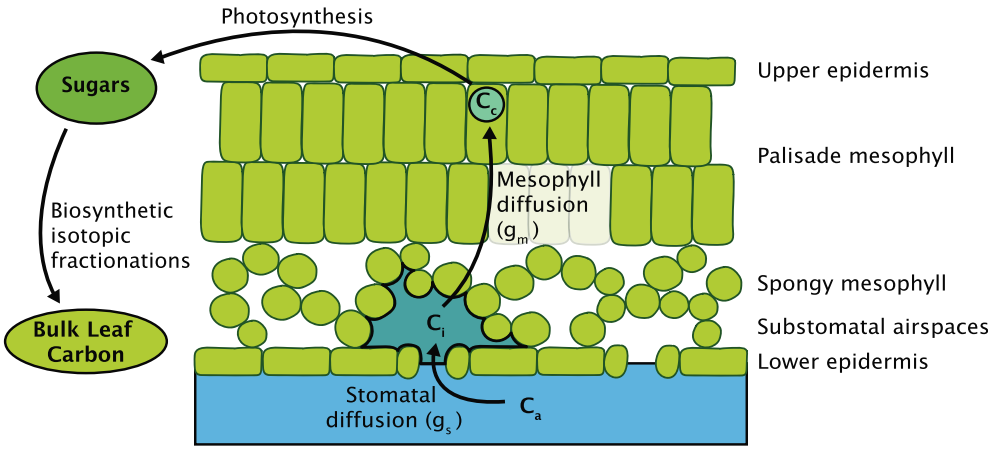

Fig. 1. Cartoon depicting the movement of carbon for photosynthesis. Carbon moves from the atmosphere (c_a) to the substomatal airspaces (c_i) via stomatal diffusion (g_s) (which imparts isotopic fractionation, "a") then to the chloroplast (c_c) via mesophyll diffusion (g_m). Photosynthesis occurs in the chloroplast (which also imparts isotopic fractionation, "b"). Synthesized sugars then undergo additional isotopic fractionations as they are used to make starches, lipids, etc. The bulk leaf carbon is a mixture of these different compounds.

Schlanser et al. (2020) pointed out that the amount of CO_2 in the atmosphere changes with altitude as well as secular global change, suggesting that in order to detect secular change, discrimination should be compared only between fossil plants that grew at similar paleoelevation. Increases in O_2:CO_2 ratios and vapor pressure deficit (VPD) are both correlated with decreasing $\Delta^{13}C$, though responses vary significantly between angiosperms and gymnosperms (Hare & Lavergne, 2021). Within C3 angiosperms and gymnosperms, traits inherent to a specific taxon have sizeable effects on $\Delta^{13}C$ (Porter et al., 2019; Sheldon et al., 2019; Schlanser et al., 2020; Stein et al., 2021; Poorter et al., 2022), which have led some to argue that the relationship between $\Delta^{13}C$ and pCO_2 is affected by too many factors for discrimination to be a good proxy for pCO_2 (Schlanser et al., 2020). Additionally, after diffusing into the substomatal cavity, carbon must still diffuse through the mesophyll to reach sites of photosynthesis in the chloroplasts (Fig. 1). Once sugars are photosynthesized, biosynthetic isotopic fractionation occurs during the formation of starches, lipids, etc. that will then influence the bulk carbon isotope composition of the leaf.

In this study, a part of the Fossil Atmospheres Project, we aimed to quantify the relationship between $\Delta^{13}C_{leaf}$ and pCO_2 in *Ginkgo*. We chose *Ginkgo* because it is a genus with an extensive fossil record during the late Mesozoic and early Cenozoic periods of hothouse climate (e.g., Royer, 2003). Any relationship between pCO_2 and $\Delta^{13}C_{leaf}$ documented in the living *G. biloba* would likely be applicable to nearly identical fossil species such as *G. wyomingensis* and *G. adiantoides* (Zhou & Zheng, 2003; Golovneva, 2010; Zhou et al., 2012). Many of the studies documenting increases in $\Delta^{13}C$ with increasing pCO_2 were conducted during the anthropogenic rise in pCO_2, and therefore at values below 400 ppm, so we also examined the relationship in *G. biloba* at pCO_2 levels up to 1000 ppm, which are more relevant for reconstructing pCO_2 in hothouse periods of the Mesozoic and early Cenozoic (Foster et al., 2017; Rae et al., 2021). Further, above 400 ppm the fit of the relationship between $\Delta^{13}C$ and pCO_2 developed by Schubert & Jahren (2012) has been calibrated only with angiosperm data. Since gymnosperms on average have lower $\Delta^{13}C$ values than angiosperms (Diefendorf et al., 2010, 2011; Hare & Lavergne, 2021), it was important to document the relationship in a gymnosperm for potential application of the C3 plant proxy in periods prior to the Late Cretaceous, when angiosperms were a smaller component of global vegetation (Carvalho et al., 2021).

2. Methods

2.1. Experimental setup

Ginkgo biloba trees were planted in an experimental field surrounded by a pine-hardwood forest at the Smithsonian Environmental Research Center in Edgewater, MD. The *G. biloba* trees are all of the same variety 'Presidential Gold'; a varietal branch was grafted onto root stock of *G. biloba* by the J. Frank Schmidt & Son Co. nursery in Boring, Oregon, so the trunks and leaves are genetically identical. We used two size classes of plants. The "large trees" (up to 3 m tall) were planted in the ground using locally sourced clay-rich topsoil and have been in chambers since the spring of 2016 (n = 15). The "small trees" (started at ~ 50 cm tall; n = 20) arrived as bare-rooted whips and were potted using Espoma Organic Potting Mix, and added to the chambers in the spring of 2019. The plants were grown in open-topped chambers (Drake et al., 1989; Day et al., 2013) which allowed for daily and seasonal fluctuations in ambient light and temperature, as well as natural precipitation (Fig. 2A). There were three chambers at each CO_2 level: 1000, 800, 600, and 450 ppm (in-chamber ambient), as well as 425 ppm for unchambered ambient plots. No CO_2 was added to the in-chamber ambient plots, but effluent air from adjacent elevated chambers slightly increases the in-chamber ambient relative to unchambered ambient plots. Chambers were arranged in a randomized block design, with three rows that each contained all five treatments (Fig. 2B).

We followed standard protocols for the setup and operation of open-top chambers (Drake et al., 1989). Carbon dioxide was added to chambers at the intake of the blower fans from CO_2 dewars under pressure. We regulated the pressure to between 40 and 60 psi, delivering the approximate total pressure required for all flow meters for the atmospheric conditions of the day. CO_2 levels were

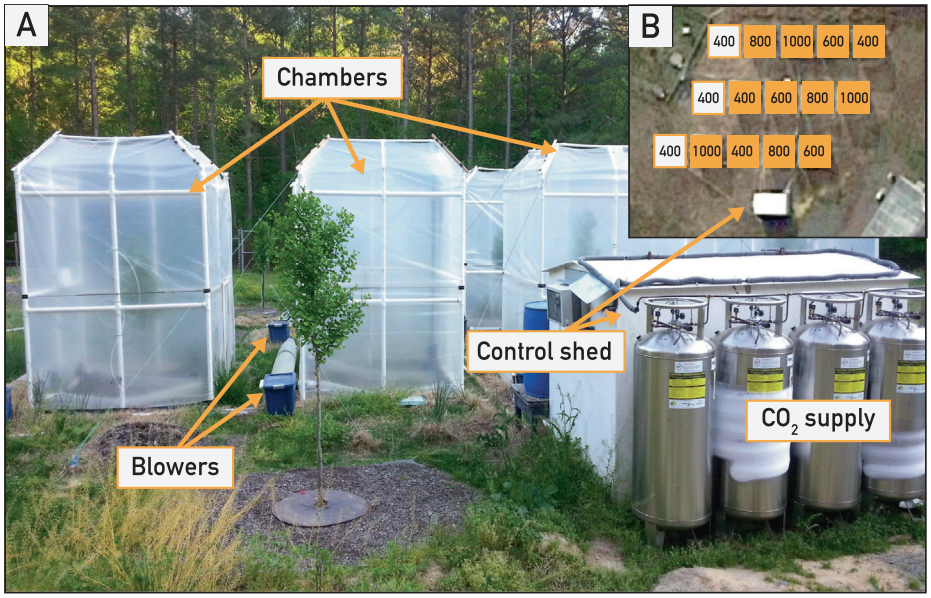

Fig. 2. (A) Experimental setup at the Smithsonian Environmental Research Center (SERC) in Edgewater, Maryland. Unchambered control tree in foreground. The control shed houses monitoring equipment as well as the supply of CO_2. Blowers combine ambient air and CO_2 from the control shed into each of the chambers. (B) The experimental plots are laid out in a randomized block design to control for plot location effects.

monitored and recorded in each chamber (or next to unchambered trees) with a single Licor 7000 gas analyzer, calibrated for CO_2 and H_2O at least 2 times per year. CO_2 levels were adjusted as needed via flowmeters in the control shed by measuring air pumped continuously back from each tree plot. A solenoid system cycled the returned air through the Licor analyzer, switching among chambers every 1.5 min and recording the value at the end before switching to the next chamber in the sequence. Human breath exhaled while moving in and out of the chambers to take measurements or perform maintenance had only a transient effect on CO_2 levels because the air inside each chamber was replaced every few minutes. Shade cloth that uniformly reflects 50 % of sunlight was added to the experiment in the summer of 2018 to equalize temperatures between chambers and unchambered controls. Plants were watered as necessary to maintain soil moisture at $\geq$ 70 % field capacity, measured using a Watermark irrometer soil moisture sensor (model 200SS-15). Plants were fertilized twice per month during the growing season with liquid Neptune Harvest organic fish and seaweed (2 N:3P:1K), and once per month with solid Espoma Plant-Tone organic (5 N:3P:3K), offset from liquid fertilizer application.

2.2. Leaf sampling and preparation

In the summers of 2018 and 2019, leaves from large trees were sampled during the first 11 and 10 weeks of the growing season, respectively, beginning when leaves were first emerging and ending $\sim$ 4 weeks after leaves had reached full expansion. In 2018, leaves were collected from both the North and South sides of the canopy. Each week, one row of trees (5 trees, one at each nominal CO_2 level) had three leaves sampled from the North and South sides of the canopy, while the remaining ten trees had one leaf sampled each from the North and South side of the tree. The row of trees subjected to extra sampling rotated each week. After observing no significant difference between leaves sampled in different canopy locations, leaves in 2019 were sampled from only the South side of the canopy (one leaf per week). Leaves were sampled from small trees every second week over the same period in the summer of 2019. All leaves sampled in the summers of 2018 and 2019 were collected from short shoots. Long shoots were not sampled. Abscised leaves were collected from the ground around the large trees in the fall of 2015 before they were planted in the experiment. In 2016–2019, all naturally abscised leaves were collected from the ground around each tree, and a subset of these were used for isotope analysis. Leaf preparation details can be found in the supplementary text.

2.3. Air sampling

Air was collected in flasks from the CO_2 source dewar and adjacent to each tree on the same day as leaf sampling in the summers of 2018 and 2019. An air pump was connected via a 15 cm long tube to a collection flask under vacuum. The pump moved air through the opened flask for a period of three minutes before being closed off.

2.4. Isotope methods

Detailed leaf and air isotope methods are provided in the supplemental text. Carbon isotope ratios of leaf samples ($\delta^{13}C_{leaf}$) were measured using elemental analysis (EA) isotope ratio mass spectrometry (IRMS). Leaves collected during the 2018 growing season were analyzed using conventional EA/IRMS at the Smithsonian Institution Museum Conservation Institute. All abscised leaves and leaves from 2019 were analyzed at the Pennsylvania State University using an EA-IRMS system modified for smaller sample size (modified EA/IRMS). About 5 mg of homogenized powder from each leaf was used for conventional isotopic analyses, and about 0.05 mg for modified EA/IRMS analyses. At both facilities, reproducibility of standards is $\leq$ 0.2 ‰ (1σ) for $\delta^{13}C$.

Atmospheric carbon dioxide samples were analyzed using OTTO-IRMS at the SIRFER lab at the University of Utah. OTTO is a custom-built sample preparation device for the analysis of CO2 from atmospheric air samples collected in 100-mL glass flasks. OTTO consists of an autosampler and a Thermo Finnigan gas chromatograph coupled to a Thermo Finnigan Delta Plus Advantage isotope ratio mass spectrometer through an open-split interface (Thermo Finnigan GC/TC); (Schauer et al., 2005). The system is run in continuous flow mode. Pure (99.999 %) carbon dioxide gas samples were analyzed for $\delta^{13}C$ and $\delta^{18}O$ using a dual inlet Thermo MAT 253 IRMS system. Oztech calibrated internal lab gas tank (pure CO_2) was used during the analyses. The Oztech tank was also calibrated against NIST standards. The measurements were comprised of twenty dual-inlet cycles.

2.5. Physiological data collection methods

Leaf gas exchange was measured using two LI-6400 Portable Photosynthesis Systems (model LI-6400XT, LI-COR Biosciences, Lincoln, NE). Plant health was determined visually: healthy plants had fully expanded, deeply green leaves, whereas unhealthy plants had smaller leaves and lighter green leaves, suggesting a lower chlorophyll concentration. Health of the plants was further confirmed by examining gas exchange data: unhealthy plants opened stomata for a briefer period, particularly during hot weather, whereas healthy plants exhibited normal ranges of stomatal conductance. Using standard techniques, we selected healthy leaves on each plant for gas exchange measurement. Measurements were made beginning one to two hours after dawn (as the day length changed from spring through fall) and before midday stomatal closure. Leaf temperatures were maintained as close to the initial value as possible using the fan in the Licor cuvette chamber. Maximum net CO_2 assimilation rate (A_{max}) was measured at saturating levels of PPFD for each plant (1000 μmol m^{-2} s^{-1}), at chamber CO_2 concentration (e.g., 400, 600, 800, or 1000 ppm), and initial flow rates were set at 500 μmol s^{-1}. Chamber relative humidity was allowed to track ambient conditions; replicate measurements performed in a random order ensured that some plants measured later in one session were measured earlier in another, and vice versa, minimizing any effect of time of day. External CO_2 concentration (c_a), was measured directly by the LI-6400, and internal CO_2 concentration (c_i) was calculated by the LI-6400 software (OPEN, LI-COR Biosciences, Lincoln, NE), as described below.

Internal CO_2 concentration (c_i; μmol CO_2 mol air^{-1}) is calculated from the following equation, derived from direct measurements of assimilation rate (A; μmol CO_2 m^{-2} s^{-1}), transpiration (E; mol H_2O m^{-2} s^{-1}), total conductance to CO_2 (g_{tc}; mol CO_2 m^{-2} s^{-1}), and mole fraction of CO_2 in the sample IRGA (C_s; μmol CO_2 mol air^{-1}):

$$c_i = \frac{(g_{tc} - \frac{E}{2})C_s - A}{g_{tc} + \frac{E}{2}}$$

The total conductance to CO_2 (g_{tc}) is derived from the stomatal conductance to water vapor (g_{sw}; mol H_2O m^{-2} s^{-1}), the boundary layer conductance to water vapor (g_{bw}; mol H_2O m^{-2} s^{-1}), and the stomatal ratio (K; dimensionless: estimate of the ratio of stomatal conductances of one side of the leaf to the other):

$$g_{tc} = \frac{1}{\left(\frac{1.6}{g_{sw}} + \frac{1.37\frac{K^2+1}{(K+1)^2}}{g_{bw}}\right)}$$

This equation uses 1.6 as the ratio of the diffusivity of CO_2 and water in air through the stomata, and 1.37 is the ratio of the diffusivity of CO_2 and water in the boundary layer (OPEN Manual, section 1–10, Li-COR Biosciences, Lincoln, NE; a full derivation of these equations and their parameters can be found within).

The c_i/c_a measurement from each tree taken on the date closest to leaf sampling in 2019 were used in this study. In the case where multiple measurements were made on the same day, the measurement with the highest c_i/c_a value was used, in order to ensure that measurements with stomata fully open were compared with one another. To process the A_{max} data, the measurements made at the very beginning and the very end of the session were deleted to remove periods of instrumental fluctuation. Measurements that recorded negative c_i values were also excluded.

2.6. Leaf mass per area (LMA) methods

Leaf mass per area was calculated for the full population of leaves collected in 2018 and 2019 (with the exception of the last week of leaves from 2018) by a simple division of the leaf mass by leaf area on an individual leaf basis. Leaves were photographed on a light box (5000 k) using a Canon EOS 5D SLR fitted with a 1:2.8 100 mm macro lens. The scale bar in the image was used for calibration in Photoshop image software. Leaf area was measured from the calibrated image using the magic wand tool, with tolerance values set to accurately capture the margin of the lamina and the complete petiole. The same leaves were dried in a Fisher Scientific oven (model 650G) at 40 °C for 48 h and then hot-massed on a Sartorius balance (model A120S) immediately after being removed from the oven. Nitrogen per unit leaf area (NPA) was also calculated using nitrogen weight % and leaf area: NPA = (N wt%/100) *LMA.

2.7. Mixing lines

Pure CO_2 was added to ambient air to raise the concentration of CO_2 within chambers. The added CO_2 had a variable carbon isotopic composition, ranging from −40.8 to −25.4 ‰ (Fig. S1), while ambient air at the site has a $\delta^{13}C_{air}$ value of ∼ -10 ‰. To calculate the isotopic composition of CO_2 in the chamber, mixing relationships between these two sources were constructed for each week of the growing season (details in supplementary text).

2.8. $\Delta^{13}C_{leaf}$ calculation

$\Delta^{13}C_{leaf}$ and $\delta^{13}C_{air}$ values were used in Eq. (2) (Farquhar et al., 1989b) for the calculation of $\Delta^{13}C_{leaf}$. In 2018, multiple leaves were collected and analyzed for $\delta^{13}C_{leaf}$ for five trees per week on a rotating basis. These measurements were averaged for one $\delta^{13}C_{leaf}$ value per tree per week. Leaf values were paired with air values from the weeks prior to collecting the leaf, assuming that a leaf collected on a given day was composed of carbon from CO_2 that had been incorporated before that collection day. For example, if the leaf was collected in week 8, then the air values from weeks 1–7 were averaged for the $\delta^{13}C_{air}$ value used in Eq. (2). We explored the possibility that carbon stored as starch from years prior to the trees being under experimental setting was used to construct leaves in 2018 and 2019 and found this not to be the case. A discussion of this topic can be found in the supplemental text, section 2.3.

2.9. Regression and ANOVA Analysis

Linear regressions were fit to $\Delta^{13}C_{leaf}$ data in Matlab (v. 9.8.0.1451342 (R2020a) Update 5) using the functions polyfit and fitlm. ANOVA analysis was used to investigate differences between nominal CO_2 groups for c_i/c_a, C:N, NPA, LMA, and A_{max} data. Analyses were carried out in Matlab using the functions anova1 and multcompare with 'Alpha' set to 0.05 for a 95 % confidence level.

2.10. Mixed effect modeling

Mixed effect modeling (MEM) was conducted in 'RStudio' (v. 4.1.0) using the lme4.0 package to investigate the importance of different factors on $\Delta^{13}C_{leaf}$. We ran two mixed effects models (MEM1 and MEM2) on each subset of our data (large trees 2018, large trees 2019, and small trees 2019) as well as all data together. The separation of data in this way avoids unequal population sizes.

We used the following model (MEM1):

$$\log(\Delta^{13}C_{leaf}) \sim pCO_2 + LMA + as.factor(chamber) + (1|Chambernumber/Treenumber) \quad (5)$$

Where "$\log(\Delta^{13}C_{leaf})$" is the log-transformed $\Delta^{13}C_{leaf}$ data, "LMA" is calculated leaf mass per area, "chamber" refers to whether the tree is chambered or unchambered ambient, and "Chambernumber/Treenumber" nests each tree's identifying number within its chamber to account for individual differences in growth environment. After identifying that growing in a chamber has a significant effect on discrimination a second model (MEM2) was run to better isolate the effect of elevated pCO_2. Two changes were made: unchambered ambient tree data were excluded, and "chamber" was removed from Eq. (5). The results from the six model runs are reported below. When running these models on all data together, two additional terms were included in both MEM1 and MEM2: +as.factor(size) and + as.factor(year), where "size" refers to small or large trees and "year" refers to 2018 or 2019.

2.11. Compilation of discrimination values from the literature

To expand the dataset for exploring the effect of pCO_2 on $\Delta^{13}C_{leaf}$, we compiled data from the literature, including recompiling data used in SJ2012. In our compilation we only included studies that calculated discrimination from leaves, that reported both $\delta^{13}C_{leaf}$ and $\delta^{13}C_{air}$, and that had at least two discrete levels of CO_2. Data from five of the eleven studies in the SJ2012 compilation satisfied these criteria, and we added data from four additional studies (Peñuelas & Azcón-Bieto, 1992; Tu et al., 2004; Hietz et al., 2005; Lomax et al., 2019); see text in supplement; data in Table S2). This is not an exhaustive literature review, but includes a range of species and plant functional types.

Species-specific differences in the relationship between pCO_2 and $\Delta^{13}C_{leaf}$ values might make it difficult to discern the overall shape of the relationship. To put data from multiple species in a common frame, we followed SJ2012 in calculating sensitivity (S, the first derivative of the curve describing the effect of pCO_2 on $\Delta^{13}C_{leaf}$). Positive S values indicated a positive relationship between $\Delta^{13}C_{leaf}$ and pCO_2; negative values the opposite. Here, we calculated S by using $\Delta^{13}C_{leaf}$ and pCO_2 values at two levels of CO_2:

$$\text{Sensitivity}\,(‰/\text{ppm}) = \frac{\Delta^{13}C_{high} - \Delta^{13}C_{low}}{pCO_{2high} - pCO_{2low}} \quad (6)$$

3. Results

3.1. Temporal trends in $\delta^{13}C_{leaf}$

Table S1 contains measurements of $\delta^{13}C_{leaf}$, $\delta^{13}C_{air}$, and pCO_2 for each of 164 leaves from which we calculated discrimination values. In 2018 and 2019, $\delta^{13}C_{leaf}$ decreased from week one to week seven of spring flush by 2.9 ± 1.4 ‰ for every tree under every level of

pCO_2 (Fig. S4). The carbon isotopic composition of leaves did not change during the last four weeks of sampling. We hypothesize that the decline and subsequent plateau of $\delta^{13}C_{leaf}$ occurs because the diffusivity of leaves, and thus c_i/c_a, increases during the spring leaf flush, as leaves expand and develop larger and more complex mesophyll airspaces, and develop larger stomata (Beck, 2009). In all subsequent analyses we used the mean $\delta^{13}C_{leaf}$ value from the last four weeks of the leaf sampling (weeks 8–12 in 2018, 7–11 in 2019; see Fig. S4) which represents the isotopic value of the fully expanded leaves. We found no significant difference between the $\delta^{13}C_{leaf}$ from each tree in the last four weeks of 2018 and senesced leaves collected in the fall of 2018 (Fig. S5), consistent with previous work finding only small differences between green leaves and leaf litter in natural settings (Graham et al., 2014; Suh & Diefendorf, 2018). Green leaves therefore give an accurate assessment of $\Delta^{13}C_{leaf}$ that can be comparable with abscised leaves and fossils.

3.2. Factors affecting $\Delta^{13}C_{leaf}$

Considering all plants, years and treatment levels, $\Delta^{13}C_{leaf}$ varied from 12.2 to 20.4 ‰, with a grand mean value of 16.1 ‰ and a standard deviation of 2.0 ‰ (Fig. 3). Variability in $\Delta^{13}C_{leaf}$ is high within each pCO_2 treatment group (range = 4.1–8.0 ‰) and also within plants of the same year-size class (2018 large, 2019 large, 2019 small) grown at the same pCO_2 level (range = 1.1–7.4 ‰). For each year-size class, the greatest mean values of $\Delta^{13}C_{leaf}$ are from the unchambered trees grown at the lowest pCO_2 (Fig. 3). Large trees in 2019 had the lowest mean values of $\Delta^{13}C_{leaf}$ at each pCO_2 treatment level. A two-way ANOVA examining the effect of year-size class and nominal pCO_2 level on $\Delta^{13}C_{leaf}$ showed a significant interaction term (8 d.f., F 2.9, p = 0.005). For this reason, analyses below are by subgroups defined by year and size as well as all together.

The results of regressions of $\Delta^{13}C_{leaf}$ versus pCO_2 by subgroup are reported in Table S2 and shown in Fig. S7. These regressions revealed only three subgroups with slopes statistically significantly different than zero ($p < 0.5$): 2018 Large trees excluding unchambered ambient trees, 2019 large trees, and 2019 small trees with slopes of 0.0036, −0.0026, −0.0027, respectively. These slopes correspond to extremely small changes in $\Delta^{13}C_{leaf}$: 0.4, −0.3, and −0.3 ‰ over 100 ppm, very close to a typical instrumental uncertainty for $\delta^{13}C$ measurements. All other subgroups gave a p value of > 0.05 for the slope estimate, so they are not significantly different from a slope of zero.

The results of the mixed effects model (MEMs) runs are shown in Table 1. Notably, all four MEM1 runs show a large proportion of variance is explained by whether trees were chambered or unchambered. This factor accounted for 31.0 %, 43.3 %, 28.2 %, and 22.0 % for 2018 large, 2019 large, 2019 small trees, and all data, respectively. In MEM2, for which unchambered tree data were removed and "chamber" was excluded from the model, LMA

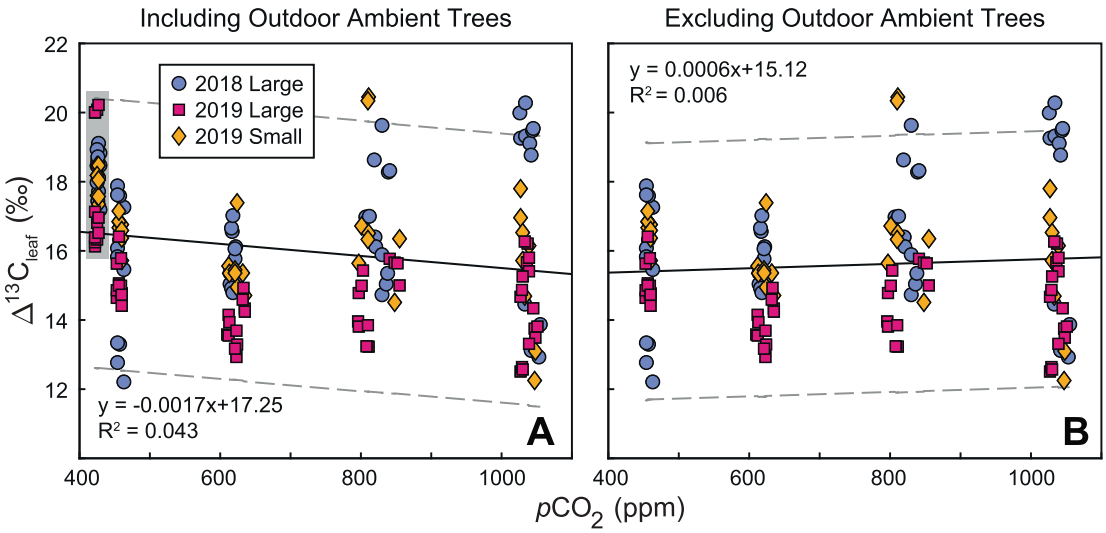

Fig. 3. Leaf-level discrimination ($\Delta^{13}C_{leaf}$) as a function of measured pCO_2. Each point represents one tree $\Delta^{13}C_{leaf}$ value for one week. For 2019, each value is from a single leaf, but for 2018 some values represent the mean of six leaves. Only the last four weeks of sampling are used. Light blue circles = large trees 2018; Magenta squares = large trees 2019; Yellow diamonds = small trees 2019. The solid black line in each panel is a linear regression through all data, the dashed grey lines are the 95 % confidence interval. (A) includes unchambered ambient trees (highlighted with shaded box). (B) unchambered trees excluded. Linear regressions give y = -0.0017x + 17.25 with an R^2 of 0.043 (A) and y = 0.0006x + 15.12 with an R^2 of 0.006 (B). Neither regression slope is significantly different from zero. Regression results (Fig. S7, Table S2) and statistics (Table S2) for subgroups are in the supplementary information file.

Table 1
Output results from eight runs of two different mixed-effects models. MEM1 includes unchambered ambient trees, while MEM2 excludes them and does not consider chamber as a variable. Values in the table represent the percent variance explained within each model run.

	2018 Large		2019 Large		2019 Small		All Data	
	MEM1	MEM2	MEM1	MEM2	MEM1	MEM2	MEM1	MEM2
Random	11.3	3.7	33.7	71.0	21.3	33.2	40.6	53.6
pCO_2	1.7	25.5	16.7	1.4	21.5	7.6	5.7	0.0
LMA	43.6	59.1	0.3	6.4	2.8	24.8	6.3	18.7
Chamber	31.0	–	43.3	–	28.2	–	22.0	–
Year	–	–	–	–	–	–	6.5	8.7
Size	–	–	–	–	–	–	2.7	4.2
Residual	12.3	11.6	6.1	21.1	26.2	34.4	16.1	14.8

accounts for a larger proportion of the variance than pCO_2 in all three datasets (59.1 to 25.5 %, 6.4 to 1.4 %, 24.8 to 7.6 %, and 18.7 to 0.0 % for 2018 large, 2019 large, and 2019 small trees, and all data, respectively).

3.3. c_i/c_a ratio and pCO_2

We examined c_i/c_a ratios measured with the LI-6400. These values are reported in Fig. 4 and Table SD2. Measured c_i/c_a ranges from 0.26 to 0.95, but an ANOVA test showed no significant differences among CO_2 groups at the 0.05 significance level.

3.4. LMA, C:N ratios, and A_{max} values

LMA, C:N, NPA, and A_{max} are plotted in Fig. 5, and values are provided in Tables SD1 and SD3. Across all plants in both years, LMA averaged 140 g/m^2 with a standard deviation of 32 g/m^2. ANOVA analysis showed LMA does not differ significantly from 425 – 600 ppm or from 800 – 1000 ppm, but there is a statistically significant increase in LMA from lower CO_2 treatment groups (425, 450, and 600 ppm) to higher treatment groups (800 and 1000 ppm) at the 0.05 significance level. The mean LMA of the lower treatment groups is 125 g/m^2, and that of the higher treatment groups is 161 g/m^2. The mean C:N ratio for all plants in both years is 32.6 with a standard deviation of 10.9. C:N ratio is not statistically significantly different between 425 and 450 ppm treatments or between 800 and 1000 ppm treatments, but there is a statistically significant increase in C:N from the 425 and 450 ppm groups to 600 ppm and from 600 ppm to 1000 ppm at the 0.05 significance level. The mean C:N of the 425 and 450 ppm group is 25.3, the mean for 600 ppm is 29.4, and the mean for the 800 and 1000 ppm group is 40.8. NPA across all plants and years averaged 2.97*10^{-4} g/m^2 with a standard deviation of 1.30*10^{-4} g/m^2. NPA of leaves from the 425 ppm treatment is significantly higher than NPA of leaves from the 450, 800, and 1000 ppm treatments, but not from those in the 600 ppm treatment. NPA in all elevated treatment levels is statistically indistinguishable. A_{max} values measured on small trees in 2019 are on average higher than values measured on large trees in the same year (mean 8.39, standard deviation 3.01 μmol•m^{-2}s^{-1}; mean 4.97, standard deviation 2.79 μmol•m^{-2}s^{-1}, respectively). There are no significant differences in A_{max} between the trees at 425 and 450 ppm nor among the three elevated treatment groups, but A_{max} of the elevated trees was significantly higher than for the two lower pCO_2 groups. (Mean A_{max} for 425 and 450 ppm trees is 7.45 μmol•m^{-2}s^{-1}, mean for elevated treatment trees is 8.98 μmol•m^{-2}s^{-1}, $p < 0.05$).

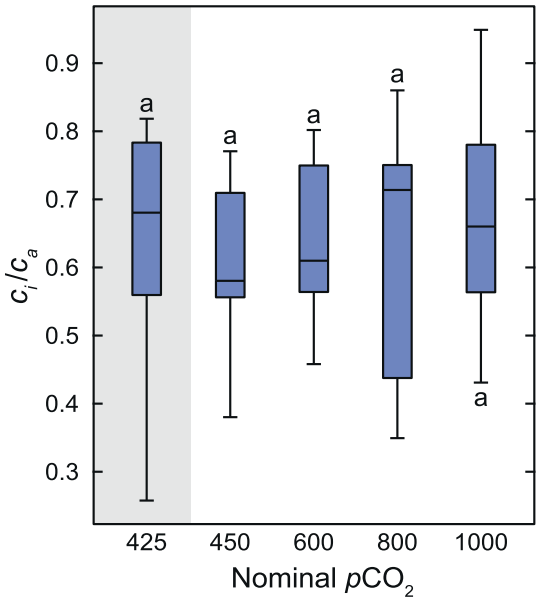

Fig. 4. Values of c_i/c_a measured by LI-6400 s for all trees in 2019. The middle marking on each box is the median value and the bottom and top edges the 25th and 75th percentiles, respectively. Whiskers extend to the largest and smallest values not considering outliers. Data for unchambered ambient trees is within the shaded area. N = 7 for each treatment.

3.5. Discrimination data compiled from the literature

Our compilation of $\Delta^{13}C_{leaf}$ values is reported, with references, in Table SD4. Sensitivity values (S) expressing the change in $\Delta^{13}C_{leaf}$ with pCO_2 are coded by growth form/plant type (Fig. 6) and range from −0.313 to + 0.194 ‰/ppm. The mean S value is 0.000 ‰/ppm, and S values near 0 are very common. The largest positive and negative values of S fall below 400 ppm, and all of the values above 500 ppm are close to zero (between −0.015 and 0.021 ‰/ppm). When coded by growth form, no trends emerge. Separating angiosperms from gymnosperms also shows no trends; both groups span nearly the full range of S values (Fig. S9).

4. Discussion

4.1. Implications of discrimination data from the literature

Our compilation of data from the literature helps to broaden evaluation of the effect of pCO_2 on $\Delta^{13}C_{leaf}$ in C3 plants. The compilation does not support a consistent relationship between sensitivity (S) and pCO_2 (Fig. 6). Instead, sensitivity values range from ~ +0.2 ‰/ppm to −0.3 ‰/ppm; opposite relationships of about equal magnitude. Sensitivity values become smaller with increasing pCO_2, indicating asymptotes in both positive and negative responses. These findings present two difficulties for the C3 plant proxy: (1) Without a consistent positive response of $\Delta^{13}C_{leaf}$ to pCO_2, the application of the C3 plant proxy to the fossil record is questionable, and (2) the asymptote in any response of $\Delta^{13}C_{leaf}$ above ~ 400 ppm CO_2 means the C3 proxy is not useful for past periods of elevated pCO_2 that are of geological interest.

How can we understand the myriad of plant responses to increasing pCO_2? We hypothesize that a combination of factors relating to plant growth strategy, taxon-specific traits, and/or environmental variables contribute to the diverse relationships between S and pCO_2. We explore these effects in the following discussion, beginning with a review on the controls of $\Delta^{13}C_{leaf}$. Then, we use our study of *Ginkgo* as a model to explore some of these factors in the context of previous work (SJ2012, SJ2018). We highlight the importance of interactions among the many factors that determine $\Delta^{13}C_{leaf}$.

4.2. Controls of $\Delta^{13}C_{leaf}$

Leaf level carbon isotope discrimination ($\Delta^{13}C_{leaf}$) is determined proximately by the balance between the rate at which CO_2 is supplied to chloroplasts and the rate at which it is consumed by carboxylation during photosynthesis (A) (Farquhar et al., 1982). The rate of supply is largely determined by atmospheric concentration of CO_2 (c_a), and the rates of diffusion through stomata (g_s) and mesophyll (g_m). The rate of photosynthesis is affected by temperature, light, and supply of CO_2, as well as biochemical and enzymatic parameters (Taiz & Zeiger, 2006). Leaf level discrimination is also influenced by the rate of photooxidation relative to photosynthesis, which is driven by temperature and O_2:CO_2 ratio (Farquhar

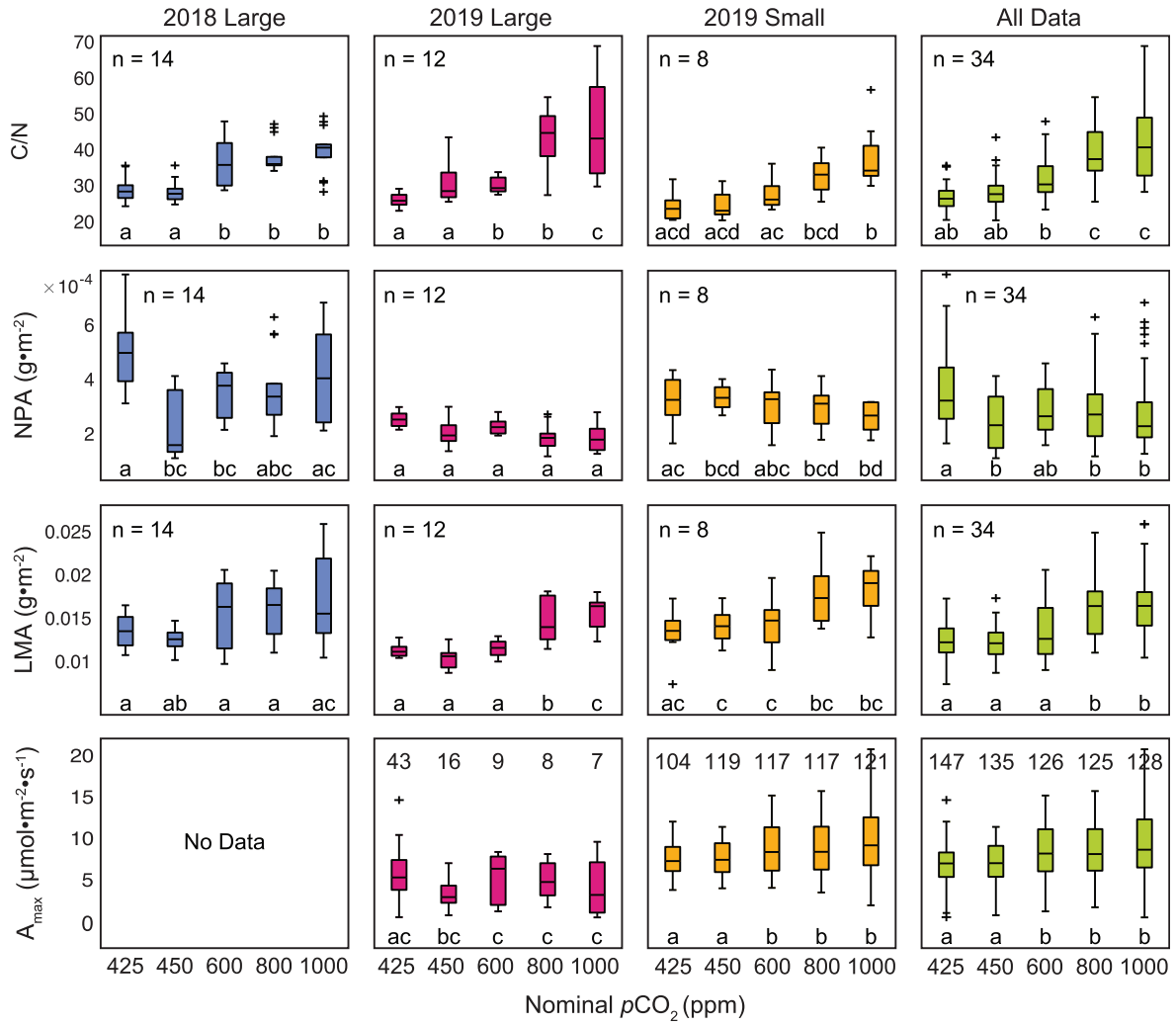

Fig. 5. Boxplots of C:N, NPA, LMA, and A_{max} values binned by nominal CO_2 level. Note, the x-axis is categorical. The middle marking on each box is the median value and the bottom and top edges the 25th and 75th percentiles, respectively. Whiskers extend to the largest and smallest values not considering outliers, which are shown as '+' marks. n = sample size. Row 1: C:N ratios. Row 2: N per unit area (NPA) in g/m^2. Row 3: Leaf mass per area (LMA) in g/m^2. Row 4: A_{max} values in µmol•m^{-2}s^{-1}, sample sizes are shown directly above each box. Column 1: Large trees, 2018, Column 2: Large trees, 2019, Column 3: Small trees, 2019, Column 4: All data. In all panels, lower case lettering indicates significant groups identified by ANOVA ($p < 0.05$).

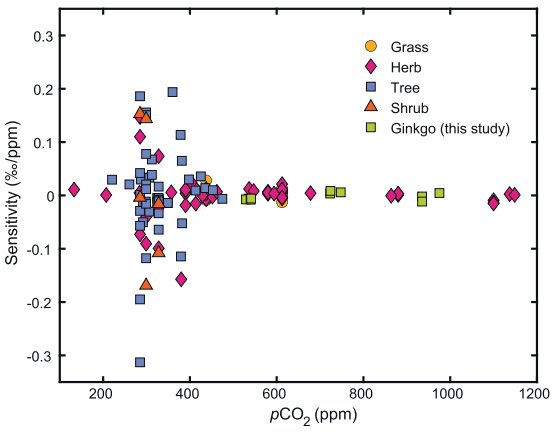

Fig. 6. Sensitivity values (S) calculated from the literature (Table SD4) and this study. Points are placed on the x-axis at the midpoint between the two CO_2 levels that were used to calculate S. Studies ranged in pCO_2 from 97 to 3000 ppm, but here we only show data up to 1200 ppm (see supplementary file for full range, Fig. S8). Plant types: grasses = yellow circles; herbs = pink diamonds; shrubs = orange triangles; trees = blue squares. *Ginkgo* values from this study are highlighted in green squares.

et al., 1982). Leaf level discrimination is generally calculated from the isotopic compositions of atmospheric CO_2 ($\delta^{13}C_{air}$) and whole leaf tissue ($\delta^{13}C_{leaf}$) according to Eq. (2); therefore, it is also possible for $\Delta^{13}C_{leaf}$ to be influenced by the proportion of different leaf tissues that have acquired different isotopic compositions during biosynthesis (e.g., lipids are commonly −4‰ and starch + 2 ‰ compared with bulk leaf; Tcherkez et al., 2011). These relationships are diagrammed in Fig. 7.

The large number of ways in which plants can respond to increased c_a permits multiple relationships between c_a and $\Delta^{13}C_{leaf}$, some of which are described in Table 2. We organize the discussion of our results below according to these scenarios. Before discussing potential effects of c_a on $\Delta^{13}C_{leaf}$, however, we point out that in mixed effects model 1 (MEM1) an important factor explaining variance in $\Delta^{13}C_{leaf}$ is whether the plant was chambered or unchambered (31.0, 43.3, 28.2, and 22.0 % of variance for 2018 Large, 2019 Large, 2019 Small trees, and all data, respectively). $\Delta^{13}C_{leaf}$ falls significantly from unchambered ambient trees (mean $\Delta^{13}C_{leaf}$ of 18.0 ‰) to chambered ambient trees (mean 15.6 ‰). Chamber effects like this have been noted in comparisons between chambered and free air carbon enrichment (FACE) studies as well (Ainsworth & Long, 2005). The chamber effect in our study is

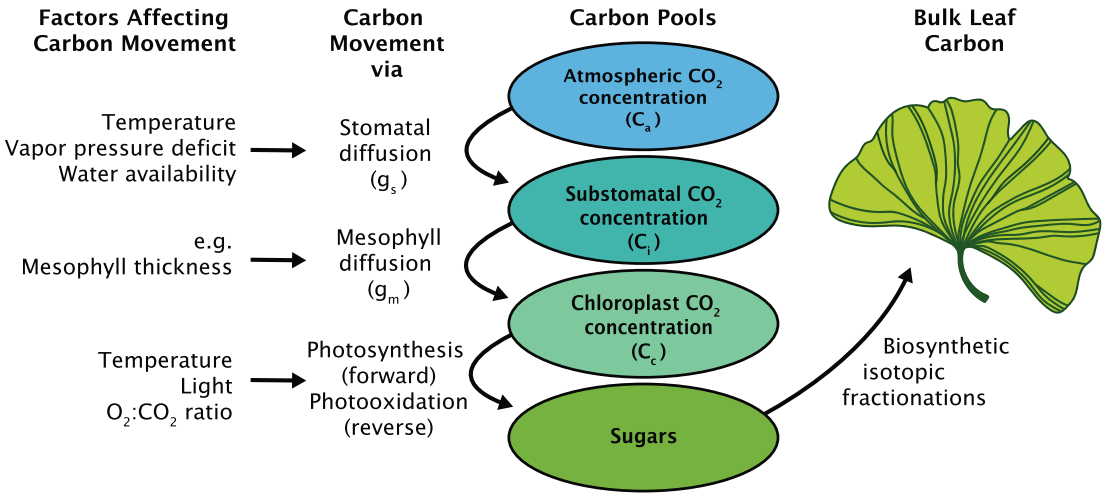

Fig. 7. Schematic of the movement of carbon between pools in the leaf and the factors that affect fluxes between pools and ultimately $\Delta^{13}C_{leaf}$. $\Delta^{13}C_{leaf}$ is calculated from $\delta^{13}C_{air}$ and $\delta^{13}C_{leaf}$ and is therefore influenced by rates of diffusion, photosynthesis, photooxidation, and isotopic fractionations that occur with each step as well as the proportion of different tissue types in the leaf. Biosynthetic fractionations are associated with the synthesis of lipids, starches, etc. The proportions of these compounds within the leaf could affect bulk $\delta^{13}C_{leaf}$.

Table 2
Responses of $\Delta^{13}C_{leaf}$ to increasing pCO_2 in SJ2012, SJ2018, and this study. Parameters fall into "Observed" or "Hypothesized" categories to explain observed $\Delta^{13}C$.

Reference	Observed			Hypothesized					Explanation
	$\Delta^{13}C_{leaf}$	A_{max}	c_i/c_a	g_s	g_m	Photo-respiration	c_i/c_a	c_c	
SJ2012	increases (hyperbolic)	–	–	increases	–	–	increases	–	Higher g_s increases c_i/c_a, permitting greater expression of RuBisCo fractionation (simplified Farquhar model)
SJ2018	increases (hyperbolic)	–	–	constant	–	decreases	constant	–	Higher internal CO_2/O_2 ratio reduces photorespiration (which would otherwise cause lower $\Delta^{13}C_{leaf}$)
This paper	unchanged	increases	unchanged	constant	decreases	not important	(observed)	constant	Decreased mesophyll conductance limits supply of CO_2 to chloroplasts, and A_{max} increases, either of which could keep C_c and $\Delta^{13}C_{leaf}$ constant.

unlikely to be related to the small increase in pCO_2 from unchambered to chambered ambient trees (32 ppm) but could be related to temperature differences between the chambers and the ambient environment.

Temperatures were on average 3.2 °C higher within than outside of chambers during the 2018 sampling season. This equates to a vapor pressure deficit (VPD) difference of 0.16 kPa (Fig. S3 panel B). Higher VPD has been shown to significantly decrease $\Delta^{13}C_{leaf}$, especially in gymnosperms, and the difference we observe in VPD would account for an ~ 1.0 ‰ drop in $\Delta^{13}C_{leaf}$ from unchambered to chambered plants (Hare & Lavergne, 2021). This effect alone is not sufficient to explain the entire difference in $\Delta^{13}C_{leaf}$ between unchambered and chambered trees. In addition to VPD changes, heightened temperatures can cause lower RuBisCO specificity, leading to higher rates of photorespiration (Tcherkez et al., 2006). Though temperature and VPD were higher in chambered than unchambered trees, they should be similar for all trees growing in chambers. Therefore, we consider the chambered trees independent of the unchambered controls to examine how $\Delta^{13}C_{leaf}$ varies with changing pCO_2 in the absence of differences in VPD.

In this study we controlled for several environmental variables. Altitude is constant across our experimental plot. By using clones, we ensured that genetic components of RuBisCO optimization do not vary (Tcherkez et al., 2006). We maintained soil moisture at or above 70 % of field capacity and regularly fertilized all plants. However, there may be residual variation in soil texture caused by differences in the topsoil used to plant the large trees. Although this may contribute to the large proportion of the variance in MEM1 explained by random effects (Chambernum:Treenum), because of the randomized block design, it should not create a false correlation between $\Delta^{13}C_{leaf}$ and pCO_2. Furthermore, the small trees planted in pots are all in the same soil type and still show high variance associated with random effects and a lack of relationship between $\Delta^{13}C_{leaf}$ and pCO_2. Once unchambered trees are removed from the analysis, all remaining trees were grown at the same temperature and VPD. When unchambered trees are removed from the mixed effect models (MEM2), the proportion of variance in $\Delta^{13}C_{leaf}$ explained by pCO_2 drops from 16.7 and 21.5 % to 1.4 and 7.6 % for 2019 large and 2019 small trees, respectively. For 2018 large trees, the proportion of variance explained by pCO_2 increases from 1.7 to 25.5 %, but LMA still explains much more variance than pCO_2 (59.1 %).

In the following sections, we consider explanations for the absence of a relationship between pCO_2 and $\Delta^{13}C_{leaf}$. These correspond to the scenarios outlined in Table 2.

4.3. Model of SJ2012: increasing c_i/c_a increases discrimination

In the model of SJ2012, increasing pCO_2 is expected to drive an increase in $\Delta^{13}C_{leaf}$ by increasing c_i/c_a and thus the internal supply of CO_2, allowing greater expression of fractionation due to RuBisCO (row 1, Table 2). We explicitly tested the SJ2012 model by using

their equation relating $\Delta^{13}C_{leaf}$ to pCO_2 (equation (6) in SJ2012) to predict known pCO_2 in our experimental trees.

$$\Delta^{13}C_{leaf} = \frac{(A)(B)(pCO_2 + C)}{(A) + (B)(pCO_2 + C)} \quad (7)$$

In Eq. (7), "A", "B", and "C" are fitting parameters determined in SJ2012 to be 28.26, 0.22, and 23.85, respectively. This equation was used to solve for pCO_2 for each value of $\Delta^{13}C_{leaf}$ from our experiment (Fig. 8).

The SJ2012 model greatly underpredicts CO_2 from $\Delta^{13}C_{leaf}$ data. Further, the CO_2 prediction residuals are trended (Fig. 8B), with the SJ2012 model increasingly underpredicting actual pCO_2 as it rises from 450 to 1000 ppm.

Although the equation of SJ2012 is a poor predictor of actual pCO_2, our results are consistent with the simplified Farquhar model upon which the SJ2012 equation is based. In the simplified Farquhar model (Eq. (1) of this paper), $\Delta^{13}C_{leaf}$ can only increase if c_i/c_a increases, since a and b are constants. Our Licor measurements indicating that c_i/c_a does not increase with pCO_2 (Fig. 3) are consistent with no change in $\Delta^{13}C_{leaf}$. We should note, however, that the physiological method of evaluating c_i/c_a has limitations. The Licor measurements are conducted over short intervals and thus may not capture the average physiological response of the plant to growth under elevated pCO_2, which is why we have focused on the mean maximum estimate for each treatment level.

We also point out that the simplified Farquhar model considers c_a as a constant (Farquhar et al., 1982, 1989a). Under constant c_a, the internal pool of CO_2 available for fixation by RuBisCO can increase only if stomatal diffusion and c_i/c_a increase. With rising c_a, however, the internal pool of CO_2 available for fixation by RuBisCO will increase even if c_i/c_a remains constant (Farquhar et al., 1982, 1989a). In other words, increasing c_a alone could increase $\Delta^{13}C_{leaf}$, contrary to Eq. (1). Given that our Licor measurements indicate constant c_i/c_a with rising CO_2, perhaps we should expect $\Delta^{13}C_{leaf}$ to increase because of a rising internal reservoir of CO_2. We explore this more in Section 4.5.

4.4. Model of SJ2018: decreasing photorespiration increases discrimination

In scenario 2 (Table 2), c_i/c_a is constant with increasing pCO_2 and a decreasing rate of photorespiration drives an increase in $\Delta^{13}C_{leaf}$. During photorespiration, O_2 reaches the active site of RuBisCO, which then acts as an oxygenase, using O_2 as a substrate. The result of this oxygenase activity is that previously fixed, ^{12}C-enriched carbon, is converted to CO_2, which can then diffuse out of the leaf. Photorespiration is therefore associated with a fractionation factor ("f"). In C3 plants, f varies from ~ 10 to 22 ‰ (Schubert & Jahren, 2018). In a second study of $\Delta^{13}C$ in *Arabidopsis*, Schubert and Jahren (2018) incorporated photorespiration into their model for inferring pCO_2 from $\Delta^{13}C$:

$$\Delta^{13}C = a + (b - a)\left(\frac{c_i}{c_a}\right) - \frac{f(\Gamma^*)}{c_a} \quad (8)$$

where Γ^* is the CO_2 compensation point in the absence of dark respiration. In Schubert and Jahren (2018), *Arabidopsis* was grown in sub-ambient CO_2 conditions where O_2:CO_2 ratios are high, increasing photorespiration. $\Delta^{13}C$ showed the same positive hyperbolic relationship with pCO_2 as in Schubert and Jahren (2012), but following Equation (8), all of the increase in $\Delta^{13}C$ was attributed to decreasing photorespiration with increasing pCO_2 at constant c_i/c_a, although no independent physiological estimates of c_i/c_a were made.

We fit the SJ2018 model to our data using values of a = 4.4 ‰, Γ^* = 80 ppm (within the range reported for *Ginkgo biloba*; (Beerling et al., 1998; Miyazawa et al., 2020)) and f = 10 ‰. Both "b" and c_i/c_a were optimized for a best fit using a least-squares fit-

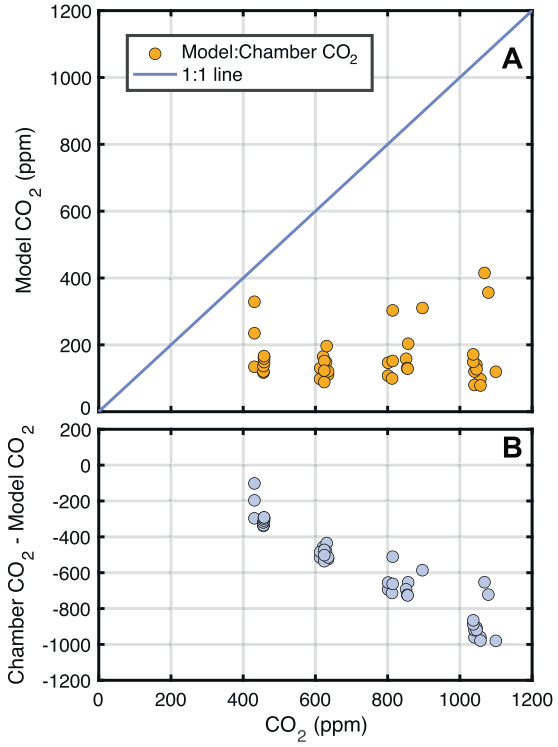

Fig. 8. (A) pCO_2 predicted by the model of SJ2012 plotted against measured pCO_2. Blue line is a 1:1 relationship. (B) Differences between predicted CO_2 and measured CO_2 values. Each point represents the mean of one tree over the last four weeks of the growing season (4 leaves per point).

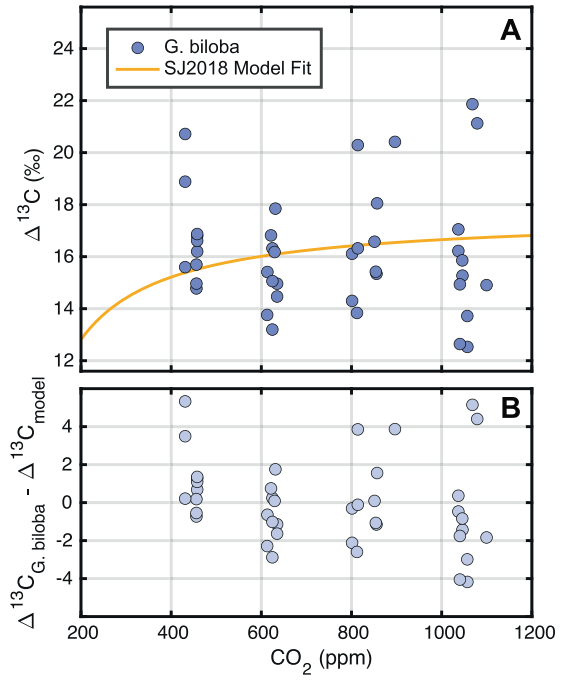

Fig. 9. (A) Observed $\Delta^{13}C_{leaf}$ compared with model of SJ2018 used to fit b and c_i/c_a with a set value of f (10‰). (B) Residuals of observed-modeled estimates of $\Delta^{13}C_{leaf}$. Each point represents the mean $\Delta^{13}C_{leaf}$ of one tree over the last four weeks of the growing season (4 leaves/point).

ting function. The best-fit result at constant c_i/c_a is shown in Fig. 9. The residuals shown in panel b are large, varying from −4 to almost 6 ‰. Residuals are also trended, with more negative residuals at higher pCO_2. The poor fit of this model to our data is not surprising; gymnosperms like *Ginkgo* have been shown to be less prone to photorespiration than angiosperms (Hare & Lavergne, 2021), so a model that relies on photorespiration as a driving mechanism for changes in $\Delta^{13}C$ is not expected to explain our data. Additionally, even the lowest levels of pCO_2 in our study (425 ppm) may be too high for photorespiration to have a measurable effect on $\Delta^{13}C_{leaf}$. (Note that pCO_2 > 400 ppm is thought to have persisted for most of the deep time periods with a hothouse climate, so the lack of a photorespiration effect under geologically relevant pCO_2 levels is important).

4.5. Model of this paper: multiple factors influence discrimination

We have seen that the models for the control of discrimination proposed by SJ2012 and SJ2018 (first two rows of Table 2) are poor predictors of the $\Delta^{13}C_{leaf}$ of *G. biloba* in our experiment. Each model implies that a single factor controls leaf-level discrimination: c_i/c_a (SJ2012) and O_2:CO_2 ratio (SJ2018). In our experiment we observed significant increases in A_{max} and LMA with increasing pCO_2 that led us to consider the role of other factors in controlling $\Delta^{13}C_{leaf}$. We hypothesize that the thicker *G. biloba* leaves that grow under elevated CO_2 may slow diffusion of CO_2 through the mesophyll from substomatal spaces (decrease g_m), thus limiting the supply and concentration of CO_2 at the sites of fixation within chloroplasts (c_c) and reducing the ability of RuBisCO to express its preference for ^{12}C. We further hypothesize that our observed ~ 20 % increase in A_{max} under elevated CO_2 results in more rapid depletion of chloroplast CO_2 supplies (c_c) and thus the ability of RuBisCO to express its preference for ^{12}C (Table 2, row 3). These changes in g_m and A_{max} would decrease the flux of CO_2 to chloroplasts while at the same time increasing rates of fixation. This would offset the effect of higher CO_2 concentration within substomatal spaces (c_i) and result in constant $\Delta^{13}C_{leaf}$ (Farquhar et al., 1982) even with rising c_a. The combination of restricting supply and increasing consumption of CO_2 in the chloroplasts prevents $\Delta^{13}C_{leaf}$ from rising. We also cannot rule out changes in bulk leaf composition such as an increase in starch that would increase $\delta^{13}C_{leaf}$ and make $\Delta^{13}C_{leaf}$ appear smaller. More generally, we should think about the expectation based on the simplified Farquhar model that c_i can only increase through an increase in g_s. This is true as long as c_a is constant, but with rising c_a, c_i will rise in proportion to c_a even with constant g_s.

If we broaden our thinking to recognize other factors aside from g_s as influencing $\Delta^{13}C_{leaf}$ (especially under increasing c_a), we then need to consider alternate explanations for constant discrimination under increasing c_a. Mesophyll conductance has received little attention in plant-based paleo-pCO_2 proxies, but is increasingly recognized as a significant factor in $\Delta^{13}C_{leaf}$, especially for gymnosperms in which mesophyll conductance is the largest single factor limiting photosynthetic rate (~40 % of the limitation on diffusion), followed by stomata and biochemistry which each account for ~ 30 % (Flexas et al., 2012; Veromann-Jürgenson et al., 2020). Other studies have found a strong positive relationship between mesophyll thickness and LMA in C3 plants (Hanba et al., 1999). Although we have not measured mesophyll conductance directly in this study, we have observed an increase in LMA in leaves grown under higher pCO_2 (Fig. 5, row 3), along with a significant increase in C:N ratio (Fig. 5, row 1). The increase in LMA and C:N ratio are consistent with an increase in structural tissue and/or starch, which would be expected to decrease total leaf diffusivity. This is consistent with the substantial proportion of variance in $\Delta^{13}C_{leaf}$ that LMA explains in our MEM2 (18.7 % for all data).

4.6. Plant growth strategy and taxon-specific traits also affect $\Delta^{13}C_{leaf}$

Voelker et al. (2016) outlined several leaf gas exchange strategies responding to increasing atmospheric CO_2 levels. Plants may (1) maintain a constant internal CO_2 level (c_i), (2) maintain a constant difference between external and internal CO_2 (c_a - c_i), (3) maintain a constant ratio of internal to external CO_2 (c_i /c_a), or (4) use a mix of strategies depending on context and the relative importance of maximizing carbon gain and minimizing H_2O loss. Though c_c is the most important quantity for understanding carbon isotope effects from photosynthesis, c_i and c_a are useful in thinking about plant carbon gain/water loss strategies that are mediated by g_s.

A constant c_a - c_i strategy may be used by herbaceous annual plants that have rapid growth and a short lifespan (Ainsworth & Long, 2005; Voelker et al., 2016), like *Arabidopsis*. This strategy values carbon gain over water loss because c_i increases with increasing c_a. Increasing c_i allows greater expression of the carbon isotope fractionation due to RuBisCO. Long-lived woody plants, particularly gymnosperms like *Ginkgo,* contain less diffusive mesophyll with thicker cell walls (Marshall & Zhang, 1994; Niinemets et al., 2009) and are more likely to maintain a constant c_i and increase water conservation as pCO_2 increases. This more conservative growth strategy would prevent $\Delta^{13}C_{leaf}$ from rising with pCO_2. Physiological measurements from this study showed that there was no significant change in c_i/c_a with increasing CO_2 in *Ginkgo* (Fig. 4), so c_i was not held constant. *Ginkgo biloba* seems to use an intermediate strategy in which water conservation is valued but carbon gain is not ignored. Reduction in mesophyll conductance further complicates $\Delta^{13}C_{leaf}$ in *Ginkgo* but may covary with plant growth strategy to produce a similar lack of change in $\Delta^{13}C_{leaf}$ with increasing pCO_2 in other woody plants with conservative growth strategies. Although growth strategies can contribute to explaining the difference between small, herbaceous plants and *Ginkgo*, there is not an obvious correlation between plant growth form and *S* in our literature compilation, and there are positive and negative values of *S* in each growth form category (Fig. 6).

Angiosperms and gymnosperms differ in attributes that cause differences in these groups' responses to increasing pCO_2. Though photorespiration was unimportant in understanding $\Delta^{13}C_{leaf}$ in this study of *Ginkgo* and for gymnosperms generally, under high O_2:CO_2 levels, photorespiration becomes increasingly important for angiosperms. Increases in VPD decrease $\Delta^{13}C_{leaf}$ in both gymnosperms and angiosperm, though the effect is larger for gymnosperms (Hare & Lavergne, 2021). When this compilation is divided into angiosperms and gymnosperms, though, we still fail to see any patterns: sensitivity values of both groups span almost the entirety of the data space (Fig. S9). Even more heterogeneity between plants can be caused by differences in RuBisCO specificity which impacts the isotope effect associated with photosynthesis; the "b" value in equation (1) is often taken to vary between 26 and 30 ‰ (Schubert and Jahren 2012), which can give several ‰ of variability in $\Delta^{13}C_{leaf}$.

4.7. Environmental factors other than pCO_2 affect $\Delta^{13}C_{leaf}$

Even if plant growth strategy, group-specific traits, and taxon-specific traits are thought to be reliably known for the fossil plants to which the C3 proxy is applied, environmental variables aside from pCO_2 are also known to have significant effects on $\Delta^{13}C_{leaf}$. Water availability has a particularly strong relationship with $\Delta^{13}C_{leaf}$, which has been demonstrated in broad geographic patterns (Diefendorf et al., 2010) as well as in controlled experiments (Lomax et al., 2019). Altitude has a strong negative relationship with $\Delta^{13}C_{leaf}$, as does VPD (Cornwell et al., 2018; Schlanser et al.,

2020; Hare & Lavergne, 2021) Soil properties such as pH and texture also have an important influence on $\Delta^{13}C_{leaf}$ via water availability (Cornwell et al., 2018). Temperature reduces RuBisCO specificity, causing increased photooxidation (Tcherkez et al., 2006). Finally, O_2:CO_2 ratios have an important influence on $\Delta^{13}C_{leaf}$ in angiosperms (Hare & Lavergne, 2021). Given the lack of a reliable paleo-O_2 proxy and uncertainties in paleo-VPD, paleoaltitude, and soil features, it appears difficult to use $\Delta^{13}C_{leaf}$ as a proxy for ancient pCO_2, even if fossils are matched for water availability and taxon-specific differences in $\Delta^{13}C_{leaf}$ are accounted for.

The compounding effects of so many factors on $\Delta^{13}C_{leaf}$—plant growth strategy, mesophyll conductance and assimilation rate, angiosperm/gymnosperm differences in response to VPD and O_2:CO_2, RuBisCO specificity—make it difficult to imagine using one relationship between pCO_2 and $\Delta^{13}C$ applied to a single plant species to reconstruct paleo-pCO_2. Some have called for an assemblage approach to the C3 plant proxy, where several types of fossil plants are used in hopes of averaging out taxon-specific effects (Porter et al., 2019). Even with this approach, uncertainty lies in reconstructing the environmental and physiological variables known to influence $\Delta^{13}C_{leaf}$. Plant responses to changing pCO_2 involve many effects that interact in different ways in different species under different conditions. The complexity, variability, and interactive nature of these effects make the reconstruction of paleo-pCO_2 from carbon isotope discrimination in C3 plants unreliable. Furthermore, the underlying model for $\Delta^{13}C_{leaf}$ response to increasing pCO_2, Eq. (1), is unfit for application to changing pCO_2 conditions, so the model used in the C3 plant proxy is fundamentally flawed.

5. Conclusions

1. In our experiment with *Ginkgo biloba*, we do not observe an increase in $\Delta^{13}C_{leaf}$ with increasing pCO_2. Our results are inconsistent with a positive hyperbolic relationship between $\Delta^{13}C_{leaf}$ and pCO_2 that could underpin a simple proxy for paleo-pCO_2 (the C3 plant proxy).
2. Likewise, we find no evidence for the changes in c_i/c_a or photorespiration that have been proposed as the underlying mechanisms for the C3 plant proxy (SJ2012 or SJ2018). Instead, we hypothesize that increasing leaf mass per area coupled with increasing assimilation rate are responsible for the lack of relationship we observed between $\Delta^{13}C_{leaf}$ and pCO_2.
3. A compilation of $\Delta^{13}C_{leaf}$ data from the literature shows no clear trend between $\Delta^{13}C_{leaf}$ and pCO_2. Responses vary widely even within plant types (herbs, trees, shrubs, grasses). $\Delta^{13}C_{leaf}$ lies at the nexus of different physiological and biochemical processes within leaves, and the most important of these processes respond to changes in water and light availability, temperature, humidity, growth strategy, and leaf anatomy and development, as well as atmospheric composition.
4. Consequently, it is unlikely that $\Delta^{13}C_{leaf}$ will consistently record atmospheric composition or any single environmental parameter. However, when the geological and botanical context of fossil leaves provide constraints on some of the environmental conditions and anatomical or physiological constraints, the isotopic composition of fossil leaves can be a powerful tool for interpreting past environmental conditions and plant function.

Data availability

Any additional data not supplied in the supplement will be made available upon request.

Declaration of Competing Interest

The authors declare that they have no known competing financial interests or personal relationships that could have appeared to influence the work reported in this paper.

Acknowledgments

We thank the Smithsonian Environmental Research Center (SERC) for logistical and technical support, with special thanks to Antoine Bercovici, Grace Cott, Andrew Peresta, Gary Peresta, and Mikayla Manyin. Many Fossil Atmospheres Project volunteers made this experiment and data collection possible. We thank the J. Frank Schmidt & Son Co. of Boring, Oregon for their generous donation of 20 whips of *Ginkgo* 'Presidential Gold'. Special thanks to Linda Davidson, Pam Hamilton, Alex Kane, Mary-Ann Pearsall, and Ryan Hinrichs for help with data collection and Gene Hunt and Erik A. Wing for advice on data analysis. We thank the Museum Conservation Institute and Christine France for isotopic measurements as well as Katherine Freeman for the use of her facilities. We thank Aaron Diefendorf, Kevin Mueller, and two anonymous reviewers of an earlier version whose comments greatly improved our manuscript. This research was funded by NSF grant EAR-1805228 (to RSB, SLW, JPW, and JPM), NSF REU Site OCE-1560088, and two grants from the Smithsonian Scholarly Studies Program.

Appendix A. Supplementary material

Supplementary material to this article can be found online at https://doi.org/10.1016/j.gca.2022.09.033.

References

Ainsworth, E.A., Long, S.P., 2005. What have we learned from 15 years of free-air CO_2 enrichment (FACE)? A meta-analytic review of the responses of photosynthesis, canopy properties and plant production to rising CO2. New Phytol. 165, 351–372.

Beck, C.B., 2009. An Introduction to Plant Structure and Development.

Beerling, D.J., McElwain, J.C., Osborne, C.P., 1998. Stomatal responses of the 'living fossil' Ginkgo biloba L. to changes in atmospheric CO_2 concentrations. J. Exp. Bot. 49, 1603–1607.

Beerling, D.J., Royer, D.L., 2011. Convergent Cenozoic CO_2 history. Nat. Geosci. 4, 418–420.

Carvalho, M.R., Jaramillo, C., de la Parra, F., Caballero-Rodríguez, D., Herrera, F., Wing, S., Turner, B.L., D'Apolito, C., Romero-Báez, M., Narváez, P., Martínez, C., Gutierrez, M., Labandeira, C., Bayona, G., Rueda, M., Paez-Reyes, M., Cárdenas, D., Duque, Á., Crowley, J.L., Santos, C., Silvestro, D., 2021. Extinction at the end-Cretaceous and the origin of modern Neotropical rainforests. Science 372, 63–68.

Cornwell, W.K., Wright, I.J., Turner, J., Maire, V., Barbour, M.M., Cernusak, L.A., Dawson, T., Ellsworth, D., Farquhar, G.D., Griffiths, H., Keitel, C., Knohl, A., Reich, P.B., Williams, D.G., Bhaskar, R., Cornelissen, J.H.C., Richards, A., Schmidt, S., Valladares, F., Körner, C., Schulze, E., Buchmann, N., Santiago, L.S., 2018. Climate and soils together regulate photosynthetic carbon isotope discrimination within C3 plants worldwide. Glob. Ecol. Biogeogr. 27, 1056–1067.

Cui, Y., Schubert, B.A., 2017. Atmospheric pCO_2 reconstructed across five early Eocene global warming events. Earth Planet. Sci. Lett. 478, 225–233.

Cui, Y., Schubert, B.A., Jahren, A.H., 2020. A 23 m.y. record of low atmospheric CO_2. Geology 48, 888–892.

Day, F.P., Schroeder, R.E., Stover, D.B., Brown, A.L.P., Butnor, J.R., Dilustro, J., Hungate, B.A., Dijkstra, P., Duval, B.D., Seiler, T.J., Drake, B.G., Hinkle, C.R., 2013. The effects of 11 yr of CO_2 enrichment on roots in a Florida scrub-oak ecosystem. New Phytol. 200, 778–787.

Diefendorf, A.F., Mueller, K.E., ScottL, W., Koch, P.L., Freeman, K.H., 2010. Global patterns in leaf ^{13}C discrimination and implications for studies of past and future climate. Proc. Natl. Acad. Sci. 107, 5738–5743.

Diefendorf, A.F., Freeman, K.H., Wing, S.L., Graham, H.V., 2011. Production of n-alkyl lipids in living plants and implications for the geologic past. Geochim. Cosmochim. Acta 75, 7472–7485.

Drake, B.G., Leadley, P.W., Arp, W.J., Nassiry, D., Curtis, P.S., 1989. An Open Top Chamber for Field Studies of Elevated Atmospheric CO_2 Concentration on Saltmarsh Vegetation. Funct. Ecol. 3, 363.

Farquhar, G.D., Ehleringer, J.R., Hubick, K.T., 1989a. Carbon Isotope Discrimination and Photosynthesis. Annual Review of Plant Physiology and Plant Molecular Biology 40, 503–537.
Farquhar, G.D., Hubick, K.T., Condon, A.G., Richards, R.A., 1989b. Stable Isotopes in Ecological Research. Ecological Studies, 21–40.
Farquhar, G., O'Leary, M., Berry, J., 1982. On the Relationship Between Carbon Isotope Discrimination and the Intercellular Carbon Dioxide Concentration in Leaves. Funct. Plant Biol. 9, 121–137.
Farquhar, G.D., von Caemmerer, S., Berry, J.A., 1980. A biochemical model of photosynthetic CO_2 assimilation in leaves of C3 species. Planta 149, 78–90.
Flexas, J., Barbour, M.M., Brendel, O., Cabrera, H.M., Carriquí, M., Díaz-Espejo, A., Douthe, C., Dreyer, E., Ferrio, J.P., Gago, J., Gallé, A., Galmés, J., Kodama, N., Medrano, H., Niinemets, Ü., Peguero-Pina, J.J., Pou, A., Ribas-Carbó, M., Tomás, M., Tosens, T., Warren, C.R., 2012. Mesophyll diffusion conductance to CO_2: An unappreciated central player in photosynthesis. Plant Sci. 193, 70–84.
Foster, G.L., Royer, D.L., Lunt, D.J., 2017. Future climate forcing potentially without precedent in the last 420 million years. Nat. Commun. 8, 14845.
Golovneva, L.B., 2010. Variability in epidermal characters of Ginkgo tzagajanica Samylina (Ginkgoales) from the Paleocene of the Tsagayan formation (Amur Region) and the taxonomy of tertiary species of Ginkgo. Paleontolog. J. 44, 584–594.
Graham, H.V., Patzkowsky, M.E., Wing, S.L., Parker, G.G., Fogel, M.L., Freeman, K.H., 2014. Isotopic characteristics of canopies in simulated leaf assemblages. Geochim. Cosmochim. Acta 144, 82–95.
Hanba, Y.T., Miyazawa, S.-I., Terashima, I., 1999. The influence of leaf thickness on the CO_2 transfer conductance and leaf stable carbon isotope ratio for some evergreen tree species in Japanese warm-temperate forests. Funct. Ecol. 13, 632–639.
Hare, V.J., Lavergne, A., 2021. Differences in carbon isotope discrimination between angiosperm and gymnosperm woody plants, and their geological significance. Geochim. Cosmochim. Acta 300, 215–230.
Lomax, B.H., Lake, J.A., Leng, M.J., Jardine, P.E., 2019. An experimental evaluation of the use of $\Delta^{13}C$ as a proxy for palaeoatmospheric CO_2. Geochim. Cosmochim. Acta 247, 162–174.
Lüthi, D., Floch, M.L., Bereiter, B., Blunier, T., Barnola, J.-M., Siegenthaler, U., Raynaud, D., Jouzel, J., Fischer, H., Kawamura, K., Stocker, T.F., 2008. High-resolution carbon dioxide concentration record 650,000–800,000 years before present. Nature 453, 379–382.
Marshall, J.D., Zhang, J., 1994. Carbon Isotope Discrimination and Water-Use Efficiency in Native Plants of the North-Central Rockies. Ecology 75, 1887–1895.
Miyazawa, S.-I., Tobita, H., Ujino-Ihara, T., Suzuki, Y., 2020. Oxygen response of leaf CO_2 compensation points used to determine Rubisco specificity factors of gymnosperm species. J. Plant. Res. 133, 205–215.
Niinemets, Ü., Díaz-Espejo, A., Flexas, J., Galmés, J., Warren, C.R., 2009. Role of mesophyll diffusion conductance in constraining potential photosynthetic productivity in the field. J. Exp. Bot. 60, 2249–2270.
Petit, J.R., Jouzel, J., Raynaud, D., Barkov, N.I., Barnola, J.-M., Basile, I., Bender, M., Chappellaz, J., Davis, M., Delaygue, G., Delmotte, M., Kotlyakov, V.M., Legrand, M., Lipenkov, V.Y., Lorius, C., Pépin, L., Ritz, C., Saltzman, E., Stievenard, M., 1999. Climate and atmospheric history of the past 420,000 years from the Vostok ice core, Antarctica. Nature 399, 429–436.
Petit, J.-R., Raynaud, D., 2020. Forty years of ice-core records of CO_2. Nature 579, 505–506.
Poorter, H., Knopf, O., Wright, I.J., Temme, A.A., Hogewoning, S.W., Graf, A., Cernusak, L.A., Pons, T.L., 2022. A meta-analysis of responses of C3 plants to atmospheric CO_2: dose–response curves for 85 traits ranging from the molecular to the whole-plant level. New Phytol. 233, 1560–1596.
Porter, A.S., Evans-Fitz, Gerald C., Yiotis, C., Montañez, I.P., McElwain, J.C., 2019. Testing the accuracy of new paleoatmospheric CO_2 proxies based on plant stable carbon isotopic composition and stomatal traits in a range of simulated paleoatmospheric O_2:CO_2 ratios. Geochim. Cosmochim. Acta 259, 69–90.
Rae, J.W.B., Zhang, Y.G., Liu, X., Foster, G.L., Stoll, H.M., Whiteford, R.D.M., 2021. Atmospheric CO_2 over the Past 66 Million Years from Marine Archives. Annu. Rev. Earth Planet. Sci. 49, 1–33.
Royer, D.L., 2003. Estimating latest Cretaceous and Tertiary atmospheric CO_2 from stomatal indices. Geol. Soc. Am. Spec. Pap. 369, 79–93.
Royer, D.L., 2015. Climate Sensitivity in the Geologic Past. Annu. Rev. Earth Planet. Sci. 44, 1–17.
Schauer, A.J., Lott, M.J., Cook, C.S., Ehleringer, J.R., 2005. An automated system for stable isotope and concentration analyses of CO2 from small atmospheric samples. Rapid Commun. Mass Spectrom. 19, 359–362.
Schlanser, K., Diefendorf, A.F., Greenwood, D.R., Mueller, K.E., West, C.K., Lowe, A.J., Basinger, J.F., Currano, E.D., Flynn, A.G., Fricke, H.C., Geng, J., Meyer, H.W., Peppe, D.J., 2020. On geologic timescales, plant carbon isotope fractionation responds to precipitation similarly to modern plants and has a small negative correlation with pCO_2. Geochim. Cosmochim. Acta 270, 264–281.
Schubert, B.A., Jahren, A.H., 2012. The effect of atmospheric CO_2 concentration on carbon isotope fractionation in C3 land plants. Geochim. Cosmochim. Acta 96, 29–43.
Schubert, B.A., Jahren, A.H., 2015. Global increase in plant carbon isotope fractionation following the Last Glacial Maximum caused by increase in atmospheric pCO_2. Geology 43, 435–438.
Schubert, B.A., Jahren, A.H., 2018. Incorporating the effects of photorespiration into terrestrial paleoclimate reconstruction. Earth Sci. Rev. 177, 637–642.
Sheldon, N.D., Smith, S.Y., Stein, R., Ng, M., 2019. Carbon isotope ecology of gymnosperms and implications for paleoclimatic and paleoecological studies. Global Planet. Change 184, 103060.
Siegenthaler, U., Stocker, T.F., Monnin, E., Lüthi, D., Schwander, J., Stauffer, B., Raynaud, D., Barnola, J.-M., Fischer, H., Masson-Delmotte, V., Jouzel, J., 2005. Stable Carbon Cycle-Climate Relationship During the Late Pleistocene. Science 310, 1313–1317.
Stein, R.A., Sheldon, N.D., Smith, S.Y., 2021. C3 plant carbon isotope discrimination does not respond to CO_2 concentration on decadal to centennial timescales. New Phytol. 229, 2576–2585.
Suh, Y.J., Diefendorf, A.F., 2018. Seasonal and canopy height variation in n-alkanes and their carbon isotopes in a temperate forest. Org Geochem. 116, 23–34.
Taiz, L., Zeiger, E., 2006. Plant Physiology. Sinauer Associates Inc..
Tcherkez, G.G.B., Farquhar, G.D., Andrews, T.J., 2006. Despite slow catalysis and confused substrate specificity, all ribulose bisphosphate carboxylases may be nearly perfectly optimized. Proc. Natl. Acad. Sci. 103, 7246–7251.
Tcherkez, G., Mahé, A., Hodges, M., 2011. $^{12}C/^{13}C$ fractionations in plant primary metabolism. Trends Plant Sci. 16, 499–506.
Veromann-Jürgenson, L.-L., Brodribb, T.J., Niinemets, Ü., Tosens, T., 2020. Pivotal Role of Mesophyll Conductance in Shaping Photosynthetic Performance across 67 Structurally Diverse Gymnosperm Species. Int. J. Plant Sci. 181, 116–128.
Voelker, S.L., Brooks, J.R., Meinzer, F.C., Anderson, R., Bader, M.K.-F., Battipaglia, G., Becklin, K.M., Beerling, D., Bert, D., Betancourt, J.L., Dawson, T.E., Domec, J., Guyette, R.P., Körner, C., Leavitt, S.W., Linder, S., Marshall, J.D., Mildner, M., Ogée, J., Panyushkina, I., Plumpton, H.J., Pregitzer, K.S., Saurer, M., Smith, A.R., Siegwolf, R.T.W., Stambaugh, M.C., Talhelm, A.F., Tardif, J.C., Water, P.K.V. de, Ward, J.K., Wingate, L., 2016. A dynamic leaf gas-exchange strategy is conserved in woody plants under changing ambient CO_2: evidence from carbon isotope discrimination in paleo and CO_2 enrichment studies. Glob. Change Biol. 22, 889–902.
Westerhold, T., Marwan, N., Drury, A.J., Liebrand, D., Agnini, C., Anagnostou, E., Barnet, J.S.K., Bohaty, S.M., Vleeschouwer, D.D., Florindo, F., Frederichs, T., Hodell, D.A., Holbourn, A.E., Kroon, D., Lauretano, V., Littler, K., Lourens, L.J., Lyle, M., Pälike, H., Röhl, U., Tian, J., Wilkens, R.H., Wilson, P.A., Zachos, J.C., 2020. An astronomically dated record of Earth's climate and its predictability over the last 66 million years. Science 369, 1383–1387.
Wu, Y., Chu, D., Tong, J., Song, H., Corso, J.D., Wignall, P.B., Song, H., Du, Y., Cui, Y., 2021. Six-fold increase of atmospheric pCO_2 during the Permian-Triassic mass extinction. Nat. Commun. 12, 2137.
Zhou, Z., Quan, C., Liu, Y.-S.(Christopher), 2012. Tertiary Ginkgo Ovulate Organs with Associated Leaves from North Dakota, U.S.A., and Their Evolutionary Significance. Int. J. Plant Sci. 173, 67–80.
Zhou, Z., Zheng, S., 2003. The missing link in Ginkgo evolution. Nature 423, 821–822.
Hietz, P., Wanek, W., Dünisch, O., 2005. Long-term trends in cellulose $\delta^{13}C$ and water-use efficiency of tropical Cedrela and Swietenia from Brazil. Tree Physiology 25, 745–752.
Tu, T.T.N., Kürschner, W.M., Schouten, S., Bergen, P.F.V., 2004. Leaf carbon isotope composition of fossil and extant oaks grown under differing atmospheric CO_2 levels. Palaeogeography, Palaeoclimatology, Palaeoecology 212, 199–213.
Peñuelas, J., Azcón-Bieto, J., 1992. Changes in leaf $\Delta^{13}C$ of herbarium plant species during the last 3 centuries of CO_2 increase. Plant, Cell & Environment 15, 485–489.